ELSEVIER

International Journal of Heat and Fluid Flow 22 (2001) 433–439

International Journal of HEAT AND FLUID FLOW

www.elsevier.com/locate/ijhff

Flow of a fluid near its density maximum in a differentially rotating cylinder

Chang Ho Lee [a], Jae Min Hyun [a,*], Ho Sang Kwak [b]

[a] *Department of Mechanical Engineering, Korea Advanced Institute of Science and Technology, 373-1 Kusong-dong, Yusong-gu, Taejon 305-701, South Korea*

[b] *School of Mechanical Engineering, Kumoh National University of Technology, 188 Sinpyeong-dong, Kumi-Shi, Kyeongsangbuk-do 730-701, South Korea*

Received 7 April 2000; accepted 12 December 2000

Abstract

A numerical study is made of the basic-state flow field of a fluid with a density maximum in a differentially rotating cylinder. The fluid density reaches a maximum ρ_m at temperature T_m, and a quadratic $(\rho$–$T)$ relationship is used to model the fluid behavior near T_m. The temperature at the bottom (top) endwall disk is T_B (T_T), with $\Delta T \equiv T_T - T_B > 0$, and T_m lies between T_B and T_T. The rotation rate of the bottom (top) endwall disk is $\Omega_B(\Omega_T)$, with $\varepsilon \equiv (\Omega_T - \Omega_B)/\Omega_B \ll 1$. Numerical solutions were obtained of the Navier–Stokes equations for large rotational Reynolds number and large Rayleigh number. Detailed flow and density fields are portrayed to be strongly dependent on the density inversion factor $\gamma \equiv (T_m - T_B)/(T_T - T_B)$. When $\gamma = 0$, the results are qualitatively similar to those of a usual Boussinesq fluid with a linear $(\rho$–$T)$ relationship. It is shown that a modified thermal wind relation prevails in the interior, in which the vertical shear of azimuthal velocity is balanced by the radial gradient of density. As γ increases, the overall strength of meridional circulation grows. The vertical profiles of azimuthal velocity are plotted as γ varies. The Ekman layer suction is intensified as γ increases. The behavior of average Nusselt number $\overline{Nu}$ at the bottom disk with varying γ is discussed and physical rationalizations are given.

Keywords: Rotating flow; Density inversion; Stratified flow

1. Introduction

The basic-state rotating flow of an incompressible viscous fluid in a vertically mounted circular cylinder [radius R, height H] poses a classical subject. As a specific example in this paper, fluid motion is maintained by a differential rotation of the bottom [rotation rate Ω_B] and top [rotation rate Ω_T] endwall disks. The sidewall is coupled to the bottom disk. Interest is confined to the situations of practical relevance in which the representative Ekman number $E[\equiv \mu/\rho_0\Omega_B H^2]$ is very small. Here, μ denotes the coefficient of viscosity, ρ_0 the reference density.

In the case of a homogeneous fluid, the global flow is divided into an essentially inviscid interior and boundary layers on the container walls. The interior flow is characterized by the celebrated Taylor–Proudman column, i.e., the dominant azimuthal velocity v is uniform in the axial direction. The Ekman layer of thickness $O(E^{1/2}H)$ is formed on each endwall disk, which, by means of Ekman layer suction, effectively controls the interior dynamics. On the cylindrical sidewall, a double-structured Stewartson boundary layer exists, which closes the meridional circulation. These principal features have been extensively documented (e.g., Roberts and Soward, 1978; Hopfinger, 1992). In passing, the role of Stewartson layer is passive in comparison to the active control of the interior flow by Ekman layers.

The introduction of a stable density stratification causes a qualitative alteration in the flow character. As a benchmark flow configuration, the pioneering works of Barcilon and Pedlosky (1967a,b) considered the Boussinesq fluid, for which a linear relation between density (ρ) and temperature (T) prevails, i.e.,

$$\rho = \rho_0[1 - \alpha(T - T_0)], \tag{1}$$

where α being the coefficient of thermometric expansion. The imposed stratification was effectuated by keeping the top endwall disk at a higher temperature $T_T(\equiv T_B + \Delta T)$ than the temperature at the bottom disk $T_B, \Delta T > 0$. The cylindrical sidewall was taken to be thermally insulated. The relative strength of the externally applied stratification was gauged by the stratification number $(S = N^2/\Omega_B^2 \equiv g\alpha\Delta T/H\Omega_B^2)$, which is assumed to be $S \sim O(1)$. It is noted that $N = (g\alpha\Delta T/H)^{1/2}$

* Corresponding author. Tel.: +82-42-869-3012; fax: +82-42-869-3210.

E-mail address: jmhyun@cais.kaist.ac.kr (J.M. Hyun).

0142-727X/01/$ - see front matter
PII: S0142-727X(01)00077-7

represents the Brunt–Vaisala frequency based on the overall imposed stable stratification. The elaborate theoretical developments of Barcilon and Pedlosky clarified the major features which are modified by the introduction of stratification. The Taylor–Proudman column is no longer sustained, and the role of Ekman-layer suction weakens or vanishes. The qualitative essentials of these rotating and stratified flows have also been illustrated in laboratory experiments (e.g., Linden, 1977).

It is emphasized here that the foregoing analytical descriptions were based on the afore-mentioned Boussinesq assumption Eq. (1) linking ρ and T in a linear relationship. However, for some fluids within a certain temperature range, density becomes maximum ρ_m at a particular temperature T_m, and ρ decreases as T deviates from T_m in both directions. In this situation, the conventional Boussinesq-fluid linear $(\rho - T)$ relation fails to adequately depict the density behavior near T_m. The convective flow characteristics of such fluids near T_m in a non-rotating container, with the temperatures at the boundary walls straddling T_m, have been addressed (e.g., Robillard and Vasseur, 1982; Braga and Viskanta, 1992; Nishimura et al., 1995; Kwak et al., 1998). The flow features of a non-Boussinesq fluid, having maximum density at T_m, in a rotating container have not been portrayed in sufficient detail, and they constitute the content of the present paper. Numerical investigations are made in this paper of steady basic-state flows in a differentially rotating cylindrical vessel. The temperature T_m, which gives rise to maximum fluid density ρ_m, lies between T_B and T_T. The thrust is given to delineating the qualitative flow character and heat transfer properties of such a non-Boussinesq fluid near T_m in a strongly rotating environment.

2. The model

A vertically mounted cylinder, filled with an incompressible viscous fluid, executes a steady differential rotation, as described earlier. The difference in rotation rate, $\Delta\Omega = \Omega_T - \Omega_B$, is very small in comparison to Ω_B. The geometrical layout, together with the cylindrical coordinates (r, ϕ, z), is sketched in Fig. 1.

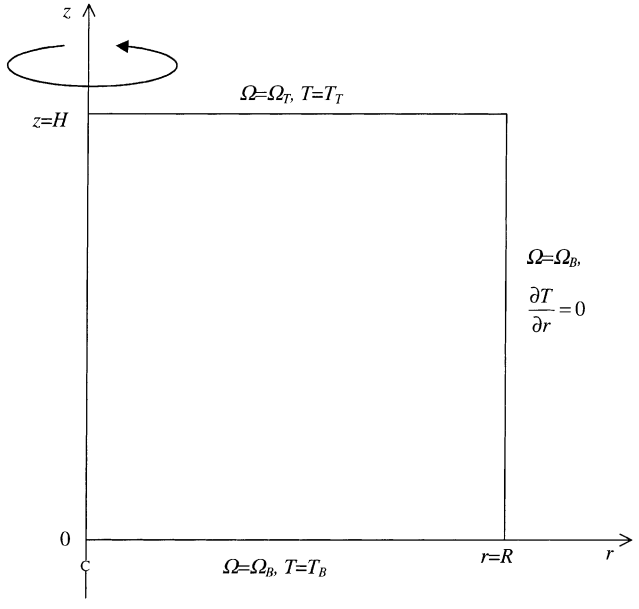

Fig. 1. Geometric configuration and coordinates.

To model the non-Boussinesq fluid having density maximum ρ_m at temperature T_m, a parabolic ρ–T relationship is adopted in the vicinity of T_m (e.g., Moore and Weiss, 1973):

$$\rho = \rho_m \left[1 - \beta (T - T_m)^2\right]. \tag{2}$$

In the case of water, the error associated with Eq. (2), with $\beta = 8.0 \times 10^{-6} (^\circ C)^{-2}$, $T_m = 3.98^\circ C$, is known to be smaller than 4% in the range from 0°C to 8°C. In the present problem setting, the overall temperature range is assumed to lie within the bound in which Eq. (2) is applicable to a high degree of accuracy. The other physical properties of the fluid are taken to be constant at T_m.

The governing, non-dimensionalized, steady, axisymmetric Navier–Stokes equations, written in the cylindrical frame (r, ϕ, z) with corresponding velocity components (u, v, w), which rotates at Ω_B, are:

$$\frac{1}{r}\frac{\partial (ru)}{\partial r} + \frac{\partial w}{\partial z} = 0, \tag{3}$$

$$u\frac{\partial u}{\partial r} + w\frac{\partial u}{\partial z} - \left(2 + \frac{v}{r}\right)v = -\frac{\partial p}{\partial r} + \frac{1}{Re}\left[\nabla^2 u - \frac{u}{r^2}\right], \tag{4}$$

$$u\frac{\partial v}{\partial r} + w\frac{\partial v}{\partial z} + \left(2 + \frac{v}{r}\right)u = \frac{1}{Re}\left[\nabla^2 v - \frac{v}{r^2}\right], \tag{5}$$

$$u\frac{\partial w}{\partial r} + w\frac{\partial w}{\partial z} = -\frac{\partial p}{\partial z} + \frac{Ra}{Re^2 Pr}(\theta - \gamma)^2 + \frac{1}{Re}\nabla^2 w, \tag{6}$$

$$u\frac{\partial \theta}{\partial r} + w\frac{\partial \theta}{\partial z} = \frac{1}{Re\,Pr}\nabla^2 \theta, \tag{7}$$

in which

$$\nabla^2 = \frac{1}{r}\frac{\partial}{\partial r}\left(r\frac{\partial}{\partial r}\right) + \frac{\partial^2}{\partial z^2}.$$

In the above, non-dimensionalization was performed by selecting R, $R\Omega_B$ and $\rho_m (R\Omega_B)^2$ for scales for length, velocity and pressure, respectively. The dimensionless temperature θ is defined $\theta = (T - T_B)/(T_T - T_B)$.

The dimensionless parameters that emerge in the equations are:

$\gamma \equiv (T_m - T_B)/(T_T - T_B)$,	density inversion factor,
$Re \equiv \rho_m \Omega_B R^2/\mu$	rotational Reynolds number,
$Ra \equiv \beta g (T_T - T_B)^2 R^3/\nu\kappa$,	Rayleigh number,
$Pr \equiv \nu/\kappa$	Prandtl number,
$\varepsilon \equiv (\Omega_T - \Omega_B)/\Omega_B$	Rossby number,

in which g, ν, and κ refer to the acceleration of gravity, kinematic viscosity, and thermal diffusivity, respectively. In the present model development, the nature of non-Boussinesq fluid is characterized by the density inversion factor γ.

The pertinent boundary conditions are

$$u = v = w = 0, \quad \theta = 0 \quad \text{at } z = 0, \tag{8a}$$

$$u = w = 0, \quad v = \epsilon r, \quad \theta = 1 \quad \text{at } z = H/R, \tag{8b}$$

$$u = v = w = 0, \quad \frac{\partial \theta}{\partial r} = 0 \quad \text{at } r = 1, \tag{8c}$$

$$u = \frac{\partial (v/r)}{\partial r} = \frac{\partial w}{\partial r} = 0, \quad \frac{\partial \theta}{\partial r} = 0 \quad \text{at } r = r_i. \tag{8d}$$

In (8d), in order to deal with the singularity at the axis $(r = 0)$, a small, finite-radius inner cylinder $(r = r_i)$ is introduced, where the symmetry condition is imposed. The value of r_i is determined on a trial-and-error basis. The use of such a fictitious inner cylinder has been shown to produce an effective and stable numerical computational procedure in rotating flows (see, e.g., Warn-Varnas et al., 1978; Hyun et al., 1982).

The assembly of equations is solved by using the finite-volume method, following the well-established procedures of SIMPLER algorithm (Patankar, 1980), together with the QUICK scheme (Hayase et al., 1992). The majority of calculations were conducted by deploying a mesh of (60×60) staggered grid points in the $(r$–$z)$ domain. Grid stretching was implemented to cluster the grid points near the solid boundaries. At least 5 grid points were placed inside the Ekman boundary layer. Grid convergence tests were carried out by using (60×60), (80×80), (100×100) meshes, and the computed results differed less than 0.1%. In order to gauge the effect of r_i, results were secured for varying values of r_i $[r_i = 0.001, 0.005, 0.01]$. The computed data at a typical interior point, e.g., at mid-radius and mid-height, differed less than 0.1%. In the ensuing computations, $r_i = 0.005$ was chosen.

Remarks are in order for the assumption of axisymmetry of flow in the present treatment. The imposition of unstable stratification, among others, may bring forth azimuthal variations, which lead to fully three-dimensional flow patterns. Determination of the appropriate regime diagrams requires a formal stability analysis of the basic-state axisymmetric flow, and the purpose of the present study is to describe such basic-state axisymmetric flow. The basic-state flow will be perturbed by an azimuthally varying disturbance, and subsequent growth/attenuation of the disturbance will be examined. An accurate portrayal of the basic-state axisymmetric flow is therefore essential, and the present numerical endeavors intend to provide such solutions.

3. Results and discussion

For all the results reported here, with a view toward simulating water near $T = 3.98$°C, the Prandtl number was set $Pr = 11.573$. The cylinder aspect ratio was $H/R = 1.0$, and the Rossby number $\varepsilon = 0.05$. As stated previously, the rotational Reynolds number Re was set to be sufficiently large to render a boundary layer-type flow.

Illustrative results are displayed in Fig. 2, which demonstrate the changes in flow character as the density inversion factor γ varies. Shown in Fig. 2 are the meridional stream function ψ, azimuthal velocity v, and the normalized density $\rho' \equiv (\rho - \rho_m)/\rho_m$, in which ψ is defined such that

$$u = \frac{1}{r}\frac{\partial \psi}{\partial z} \quad \text{and} \quad w = -\frac{1}{r}\frac{\partial \psi}{\partial r}.$$

In the case of $\gamma = 0$ (see Fig. 2(c)), for which $T_B = T_m$, the overall velocity patterns are akin to those of a stably stratified Boussinesq fluid [Fig. 2(b)]. The meridional flow forms a clockwise circulating cell. The flow is vigorous in the boundary layers, and in the interior at small and moderate radii the meridional flow weakens. The azimuthal velocity field in the interior has weak vertical shears. These features are qualitatively similar to the analytical findings elaborated by Barcilon and Pedlosky (1967a,b) for a Boussinesq fluid. However, the main difference is seen in the density field. The fact that the density at the bottom (top) is maximum (minimum) is qualitatively similar to the case of a Boussinesq fluid. The density in the bottom left region of the meridional plane is nearly equal to ρ_m, and in the top right region the fluid is stably stratified. It is also obvious that, for the non-Boussinesq fluid, the classical thermal wind relation, i.e.,

$$\frac{\partial v}{\partial z} = \frac{Ra}{2Re^2 Pr}\frac{\partial \theta}{\partial r},$$

which is valid in the interior for a Boussinesq fluid, does not hold. As stipulated in Barcilon and Pedlosky (1967a,b), the thermal wind relation for a Boussinesq fluid points to the balance between vertical shear of azimuthal velocity and horizontal gradient of temperature.

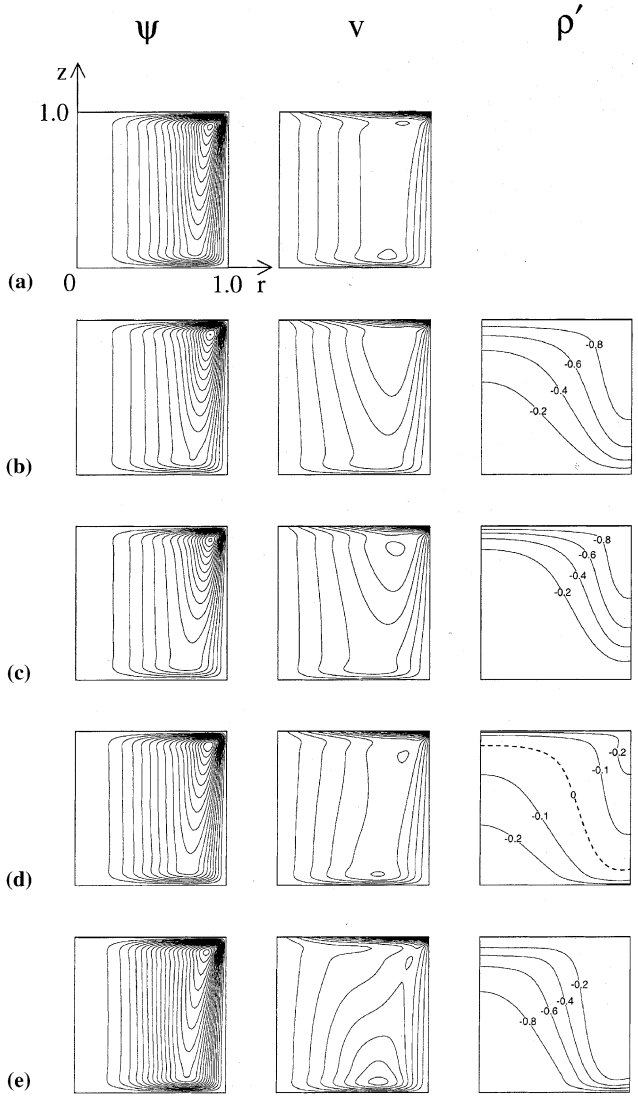

Fig. 2. Plots of ψ, v and $\rho' \equiv (\rho - \rho_m)/\rho_m$ in the meridional plane. Conditions are $Re = 1000$ and $Ra = 2 \times 10^5$. The contour increments are $\Delta\psi = 2.2 \times 10^{-5}$ and $\Delta v = 3.1 \times 10^{-3}$. The dotted line in density plots denotes the ρ_m-line: (a) Homogeneous fluid, $|\psi_{max}| = 4.26 \times 10^{-4}$; (b) Boussinesq fluid, $|\psi_{max}| = 3.74 \times 10^{-4}$; (c)–(e): non-Boussinesq fluids; (c) $\gamma = 0$, $|\psi_{max}| = 3.55 \times 10^{-4}$; (d) $\gamma = 0.5$, $|\psi_{max}| = 3.95 \times 10^{-4}$; (e) $\gamma = 1.0$, $|\psi_{max}| = 4.48 \times 10^{-4}$.

In order to examine the flow behavior in further detail, the individual terms in the equation for azimuthal vorticity

$$\eta\left[\equiv \frac{\partial u}{\partial z} - \frac{\partial w}{\partial r}\right]$$

are compared i.e.,

$$0 = \underbrace{-u\left(\frac{\partial \eta}{\partial r} - \frac{\eta}{r}\right) - w\frac{\partial \eta}{\partial z}}_{\text{(I)}} + \underbrace{\frac{\partial}{\partial z}\left(\frac{v^2}{r}\right)}_{\text{(II)}} + \underbrace{2\frac{\partial v}{\partial z}}_{\text{(III)}} + \underbrace{\frac{1}{Re}\left[\frac{\partial}{\partial r}\left(\frac{\partial r\eta}{r\partial r}\right) + \frac{\partial^2 \eta}{\partial z^2}\right]}_{\text{(IV)}} - \underbrace{\frac{Ra}{Re^2 Pr}\frac{\partial}{\partial r}(\theta - \gamma)^2}_{\text{(V)}}. \tag{9}$$

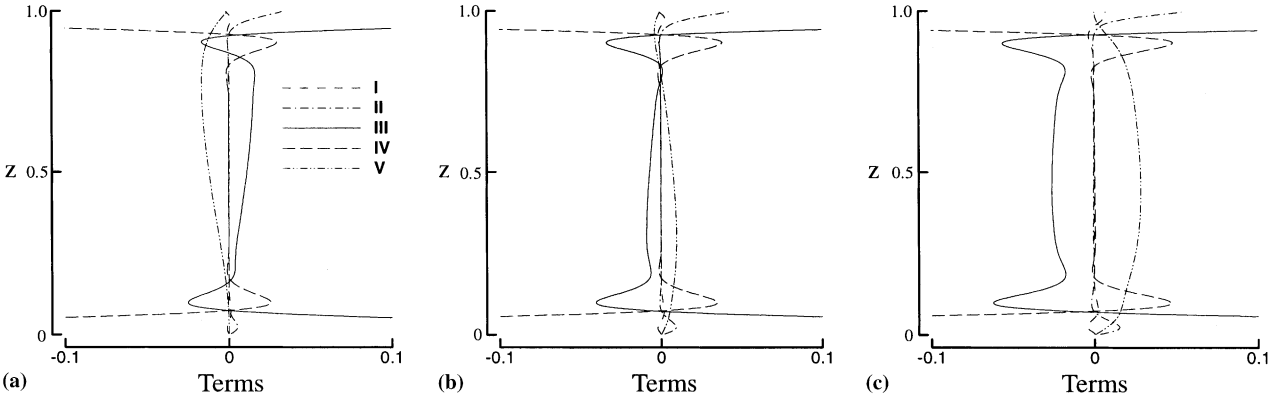

Fig. 3. Comparisons of the terms in the vorticity Eq. (9) along $r = 0.5$. Conditions are $Re = 1000$ and $Ra = 2 \times 10^5$: (a) $\gamma = 0$; (b) $\gamma = 0.5$; (c) $\gamma = 1.0$.

As is apparent in Fig. 3(a) for $\gamma = 0$, the dominant balance in the interior is between the Coriolis term (III) and the buoyancy term (V), which leads to a modified thermal wind relation for a non-Boussinesq fluid of Eq. (2):

$$\frac{\partial v}{\partial z} \cong \frac{Ra}{2Re^2 Pr} \frac{\partial}{\partial r}(\theta - \gamma)^2. \tag{10}$$

It is useful to make comparisons by inspecting the results for $\gamma = 1.0$, i.e., $T_T = T_m$, exhibited in Figs. 2(e) and 3(c). The entire cavity is in a gravitationally unstable configuration, and the qualitative pattern of density field is opposite to that of $\gamma = 0$ The strength of meridional circulation is larger than for $\gamma = 0$, and the sign of $\partial v/\partial z$ is negative in much of the cavity interior. It is stressed that the computed results represent the axisymmetric basic-state flow field. The question of whether such a flow of gravitationally-unstable configuration realistically exists may be answered by undertaking a formal stability analysis. As emphasized earlier, the objective of the present numerical study is to capture the axisymmetric flow, which will be used as the basic-state flow for stability analysis.

In the case of $\gamma = 0.5$, the maximum-density temperature T_m lies halfway between T_B and T_T. Fig. 2(d) demonstrates the iso-surface of ρ_m, stretching from the top axis zone to the lower right corner of the meridional plane. Below (above) the iso-surface of $\rho_m(\theta = \gamma)$ the density increases (decreases) upward, creating a gravitationally-unstable (stable) configuration and $\partial v/\partial z$ changes its sign on the iso-surface of ρ_m. The strength of meridional circulation is larger than that for $\gamma = 0$. The general character of azimuthal flow field and density ρ is intermediate between the extreme cases of $\gamma = 0$ and $\gamma = 1.0$. These observations are consistent with the modified thermal wind relation of Eq. (10), i.e., balance is maintained between vertical shear of azimuthal velocity and horizontal gradient of buoyancy.

Compiling numerical results, the vertical profiles of v at mid-radius ($r = 0.5$) are plotted in Fig. 4. Clearly, as γ varies, the changes in the vertical shear of azimuthal velocity $\partial v/\partial z$ in the interior are discernible. The sign of $\partial v/\partial z$ is positive for $\gamma = 0$, but as γ increases, the vertical profile of v slopes in the negative direction. These qualitative patterns are in accord with the modified thermal wind relation of Eq. (10).

One significant element of rapidly rotating flows is the Ekman boundary layer. This layer is called for to adjust smoothly the dominant azimuthal flow in the inviscid interior to the no-slip condition at the endwall disk. The linearized solution for the velocity structure in the Ekman layer has been given in the textbooks (e.g., Greenspan, 1968). An important function of the Ekman layer is that an axial flow of magnitude of $O(E^{1/2}v)$, where the Ekman number $E \equiv (R/H)^2 Re^{-1}$, is

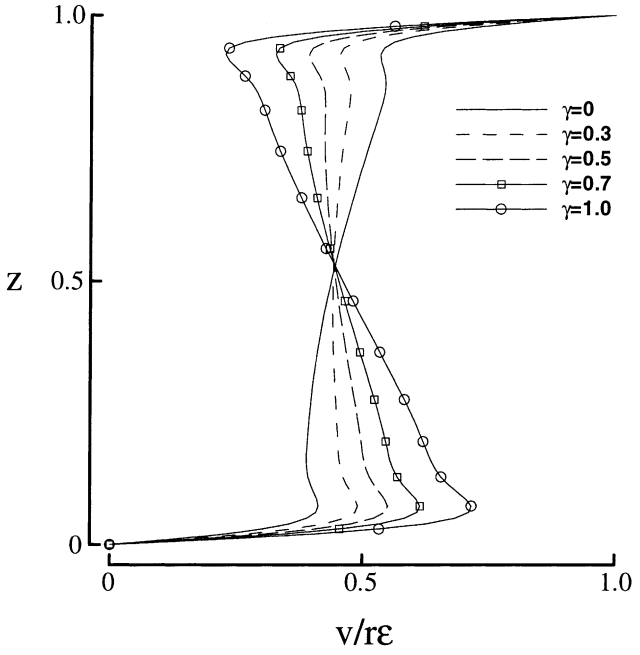

Fig. 4. Vertical distributions of azimuthal velocity v along $r = 0.5$. Conditions are $Re = 1000$ and $Ra = 2 \times 10^5$.

induced if there exists a difference in axial vorticity between the interior flow and the endwall disk. By this mechanism, the Ekman layer exerts control of the interior dynamics, which is often referred to as the Ekman suction (see, e.g., Roberts and Soward, 1978; Hopfinger, 1992). The v profiles of Fig. 4 also provide a basis to estimate the strength of Ekman suction as well as the resultant global meridional circulation. The classical treatises of Barcilon and Pedlosky (1967a,b) established that, for a stratified fluid of $S \sim O(1)$, the Ekman boundary layer suction can still be determined by the Ekman compatibility condition, i.e., the vertical velocity at the edge of Ekman layer, W_e, is

$$W_e \cong \pm \frac{1}{2} E^{1/2}(\zeta_{\text{fluid}} - \zeta_{\text{wall}}) \quad \text{at } z = 0 \text{ and } H/R, \tag{11}$$

in which ζ denotes the axial vorticity

$$\zeta \equiv \frac{1}{r} \frac{\partial (rv)}{\partial r}.$$

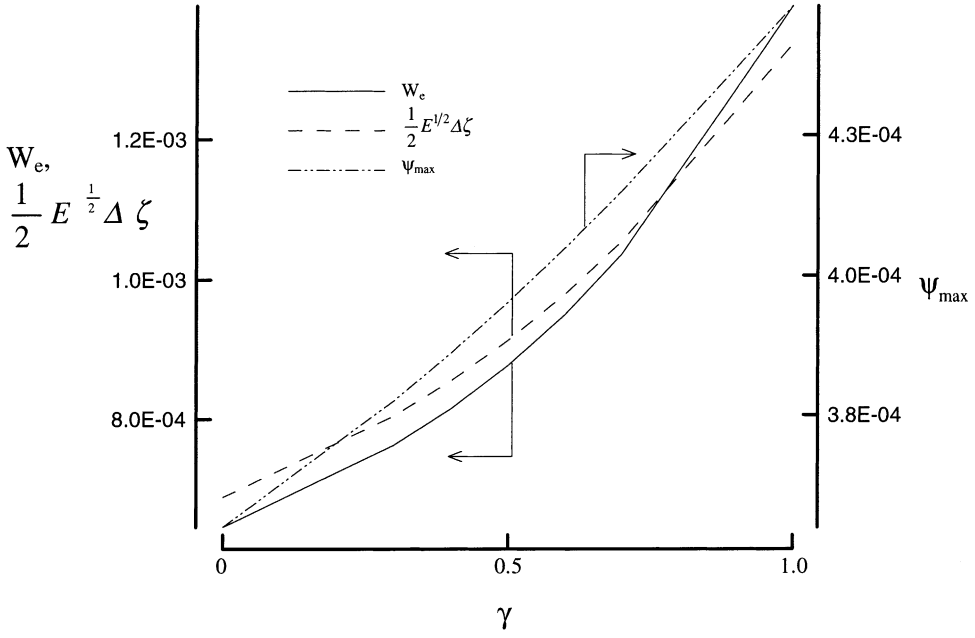

Fig. 5. Behavior of W_e at the edge of Ekman layer, Eq. (11). Also shown are $\Delta\zeta$ and ψ_{max}. Conditions are $Re = 1000$ and $Ra = 2 \times 10^5$.

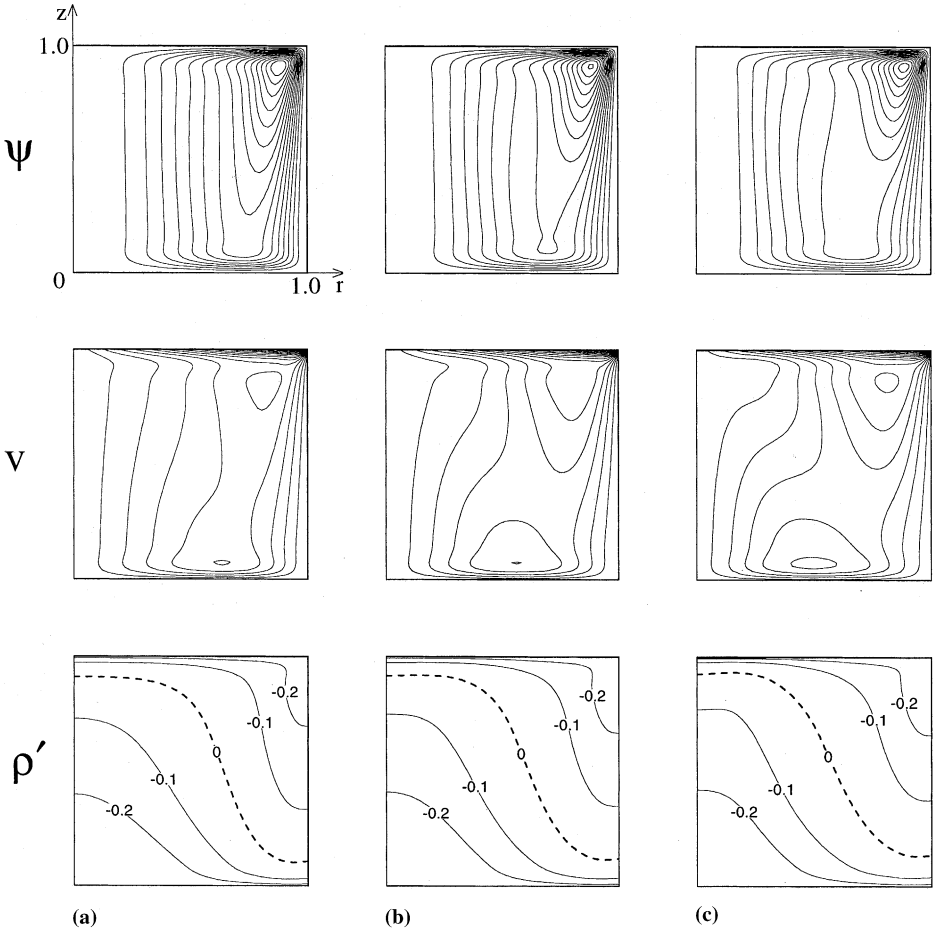

Fig. 6. Plots of ψ, v and ρ' in the meridional plane. Conditions are $Re = 1000$ and $\gamma = 0.5$. The contour increments are $\Delta\psi = 2.4 \times 10^{-5}$ and $\Delta v = 3.1 \times 10^{-3}$. The dotted line denotes the ρ_m-line: (a) $Ra = 3 \times 10^5, |\psi_{max}| = 3.83 \times 10^{-4}$; (b) $Ra = 5 \times 10^5, |\psi_{max}| 3.62 \times 10^{-4}$; (c) $Ra = 7 \times 10^5, |\psi_{max}| 3.45 \times 10^{-4}$.

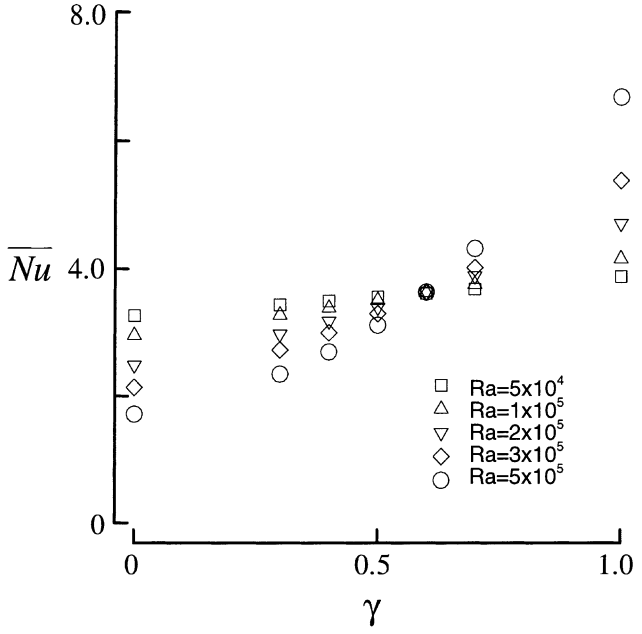

Fig. 7. Averaged Nusselt number at the bottom disk, $\overline{Nu}$.

The computed numerical results, exemplified in Fig. 5, are in close consistency with the above analytical predictions. As illustrated in Fig. 4, the magnitude of v at the edge of Ekman layer deviates further from that of the endwall disk, as γ increases. These intensified v-velocities in the Ekman layer lead to larger differences in axial vorticities between the edge of Ekman layer and the endwall disk, i.e., $(\zeta_{\text{fluid}} - \zeta_{\text{wall}})$. This, in turn, gives rise to an invigorated Ekman layer suction, which turns up in an increased value of W_e, as shown in Eq. (11). The enhanced Ekman layer suction causes the meridional circulation in the interior to grow in strength. The plots of $\psi_{\max}$ in Fig. 5 are in line with these physical interpretations.

The effect of Ra on the overall flow pattern is illustrated in Fig. 6 for the representative case $\gamma = 0.5$. It is noted that the vertical shear of azimuthal velocity, $\partial v/\partial z$, changes sign near the iso-surface of ρ_m, which is inserted in the ρ'-field plots as a dotted line. In the region of positive(negative) $\partial v/\partial z$, which is above(below) this iso-surface, the magnitude of $\partial v/\partial z$ increases as Ra increases. This reflects the fact that the global system-wide density stratification increases as Ra increases. The maximum strength of meridional circulation, which is seen near the upper right corner region, is reduced, as Ra increases, due to the stabilizing buoyancy in this area.

On the basis of the computed data, the convective heat transfer at the bottom endwall disk is calculated. For this purpose, the average Nusselt number, $\overline{Nu}$, at the bottom disk is defined as follows:

$$\overline{Nu} = \frac{R}{H}\int_0^1 \left(\frac{\partial\theta}{\partial z}\right)_{z=0} 2\pi r\,\mathrm{d}r.$$

Fig. 7 displays $\overline{Nu}$ as a function of γ for varying values of Ra. In general, $\overline{Nu}$ increases as γ increases. This is easily anticipated, since the convective activities are more vigorous as γ increases, as illustrated previously. An inspection of Fig. 7 reveals that the value $\gamma \cong 0.6$ serves as a demarcation line for the $\overline{Nu}$–γ curves. First, near $\gamma = 0.6$, the $\overline{Nu}$-values, approximately $\overline{Nu} = 3.60$, are almost independent of Ra. It is also remarked that this value is very close to the $\overline{Nu}$ value for pure forced convection of a homogeneous fluid. This implies that, for a non-Boussinesq fluid with $\gamma = 0.6$, the whole flow field is almost equally divided into a gravitationally-stable and a gravitationally-unstable region. The individual effects are comparable and offsetting each other, which produces a situation in which the net effect of buoyancy is very small. However, it is stressed that the detailed flow structures are substantially different from the case of a homogeneous fluid. The opposing dynamical influences of buoyancy, depending on $\gamma \gtrless 0.6$, are also manifested in the $\overline{Nu}$–Ra behavior. As illustrated, for $\gamma \gtrsim 0.6$, $\overline{Nu}$ increases as Ra increases, which reflects the dominant influence of buoyancy in a gravitationally-unstable configuration. For $\gamma \lesssim 0.6$, $\overline{Nu}$ decreases as Ra increases, which indicates the opposite trend.

4. Conclusion

The computed results indicate that the qualitative flow character depends crucially on the density inversion factor γ.

For a non-Boussinesq fluid with $\gamma = 0$, the general flow pattern is similar to that of a Boussinesq fluid. However, in the interior, instead of the usual thermal wind relation, a modified version should be used which reflects the non-linear $(\rho$–$T)$ relationship. For $\gamma = 1.0$, the strength of meridional circulation increases, and $\partial v/\partial z$ is negative in much of the cavity interior.

The magnitude of v at the edge of Ekman layer deviates further from that of the endwall disk, as γ increases. This enhanced Ekman layer suction invigorates the meridional circulation in the interior.

Acknowledgements

Appreciation is extended to the referees whose constructive comments led to improvements in the revised version. This work was supported by grants from MOST, KOSEF, and the NRL project, South Korea.

References

Barcilon, V., Pedlosky, J., 1967a. Linear theory of rotating stratified fluid motions. J. Fluid Mech. 29, 1–16.

Barcilon, V., Pedlosky, J., 1967b. A unified linear theory of homogeneous stratified rotating fluids. J. Fluid Mech. 29, 609–621.

Braga, S.L., Viskanta, R., 1992. Transient natural convection of water near its density extremum in a rectangular cavity. Int. J. Heat Mass Transfer 35, 861–875.

Greenspan, H.P., 1968. The Theory of Rotating Fluids. Cambridge University Press, Cambridge.

Hayase, T., Humphrey, J.A.C., Grief, R., 1992. A consistently formulated QUICK scheme for fast and stable convergence using finite-volume iterative calculation procedures. J. Comput. Phys. 98, 108–118.

Hopfinger, E.J., 1992. Rotating fluids in geophysical and industrial applications. Springer, New York.

Hyun, J.M., Fowlis, W.W., Warn-Varnas, A., 1982. Numerical solutions for the spin-up of a stratified fluid. J. Fluid Mech. 117, 71–99.

Kwak, H.S., Kuwahara, K., Hyun, J.M., 1998. Convective cool-down of a contained fluid through its maximum density temperature. Int. J. Heat Mass Transfer 41, 323–333.

Linden, P.F., 1977. The flow of a stratified fluid in a rotating annulus. J. Fluid Mech. 79, 435–447.

Moore, D.R., Weiss, N.O., 1973. Nonlinear penetrative convection. J. Fluid Mech. 61, 553–581.

Nishimura, T., Wake, A., Fukumori, E., 1995. Natural convection of water near the density extremum for a wide range of Rayleigh numbers. Numer. Heat Transfer 27, 443–449.

Patankar, S.V., 1980. Numerical Heat Transfer and Fluid Flow. McGraw-Hill, New York.

Roberts, P.H., Soward, A.M., 1978. Rotating Fluids in Geophysics. Academic press, New York.

Robillard, L., Vasseur, P., 1982. Convective response of a mass of water near 4°C to a constant cooling rate applied on its boundaries. J. Fluid Mech. 118, 123–141.

Warn-Varnas, A., Fowlis, W.W., Piacsek, S., Lee, S.M., 1978. Numerical solution and laser-Doppler measurements of spin-up. J. Fluid Mech. 85, 609–639.